

# Eddy Around Zhoushan Island: Observations with Synthetic Aperture Radar at C-band

Xianliang HUANG <sup>a,1</sup>

<sup>a</sup>*School of Marine Science and Technology, Zhejiang Ocean University, Zhoushan 316022, China*

**Abstract.** We studied mesoscale (~100 km length) eddy around the Zhoushan Island (one Sentinel-1 (S-1) image at coastal East China Sea). The simultaneous sea surface temperature (SST) data from the Advanced Very High-Resolution Radiometer (AVHRR) confirms the existence of upwelling in the Western Pacific Ocean, although, the AVHRR data around the Zhoushan Islands were not available. The difference in the root mean square error (RMSE) between the simulations with the Region Ocean Modelling System (ROMS) and that of the AVHRR data was around 1 °C. Also, the RMSE of the model-simulated current speed compared with that of the Climate Forecast System Version 2 (CFSv2) data was 0.04 m/s. We concluded that natural biogenic slicks mainly contributed to damping Bragg waves for sub-mesoscale upwelling, while ocean currents are an important factor affecting the roughness of mesoscale cold eddies.

**Keywords.** Upwelling, eddy, synthetic aperture radar, C-band

## 1. Introduction

Ocean eddy and upwelling are common ocean phenomena, which have distinguishing features of sea surface current and temperature away from surrounding waters. The characteristics of these phenomena are that there is frontal boundary area with strong horizontal and vertical velocity gradients. These are closely related with the marine ecosystem and the global climate change in various ways by heat and nutrient exchange [1]. Operational product, such as SST measured by an Advanced Very High-Resolution Radiometer (AVHRR), has been popularly used by the ocean colour remote sensing community to monitor ocean eddy and upwelling events [2, 3]. However, the optical images are fuzzy, and the information of earth objects cannot be read due to clouds associated with increased biological activity in upwelling regions from the remote sensing images [4]. Moreover, sea surface current is also undetectable from optical satellite imagery.

Microwave Synthetic Aperture Radars (SAR) are efficient instruments for all-weather high-resolution remote sensing of the sea surface. In particular, SAR has the capability for sea surface monitoring under extreme conditions [5, 6]. Satellites carrying SARs operating at C-band (5.3 GHz) include ERS-1/2, RADARSAT-1/2 (R-

---

<sup>1</sup> Xianliang Huang, School of Marine Science and Technology, Zhejiang Ocean University, Zhoushan 316022, China; E-mail: sherlingh@163.com.

1/2), and Sentinel-1A/1B (S-1). The intensity of the reflected signal detected by SAR is determined by the roughness of the sea surface. The roughness of the sea surface is related to the distribution of the Bragg backscattered waves on the sea surface, and depends on various processes such as wind, surface waves, topography, ocean currents, fronts and internal waves. [7, 8]. For example, observed an obvious oceanfront in an L-band SeaSAT-SAR image, due to fine resolution and good real-time performance [9].

The processes of the sea surface long waves, atmospheric circulation and ocean currents may modulate the Bragg wave spectrum [10, 11]. In the past few decades, various mechanisms of SAR surge sensing have been studied, including modulation of divergence and convergence caused by sea currents [12]; the instability of the sea-atmosphere boundary layer caused by sea temperature [13]; and the change of surface viscosity caused by the low temperature of upwelled waters [14]. The local upwelling is generated by multiple factors, including wind, bathymetry, tidal mixing, and Kuroshio current around the Zhoushan island.

This study is organized into five sections. Section 1 investigates the possibility of upwelling studies with C-band SARs, namely S-1. It introduces the available datasets, including NCEP climate forecast system version 2 (CFSv2) ocean current, images of SAR, the European Centre for Medium-Range Weather Forecasts (ECMWF) wind data, and SST from AVHRRs flown on NOAA satellites in the Section 2; it describes dynamic parameters dependence on the SAR-derived normalized radar cross (NRCS) in upwelling dominated regions, and Section 4 describes how we tuned an empirical function to relate the variation of NRCS with wind speed and SST. Finally, section five summarizes the conclusions of the study.

## 2. Data Source

One C-band vertical-vertical (VV) polarization SAR images were analyzed. S-1 images taken at 09:45 UTC on November 12, 2015, in interferometric wide-swath (IW) around the Zhoushan Island were acquired with a size of  $20 \text{ m} \times 5 \text{ m}$  pixel in the along-track /cross-track directions, respectively. Figure 1 shows the S-1 images after calibration, and the weak backscattering is obvious. An ocean numerical model, called Region Ocean Modeling System (ROMS), was employed to simulate current fields in the East China Sea and the South China Sea ( $76.6^\circ \text{ E}$  to  $160^\circ \text{ E}$ ,  $20.5^\circ \text{ S}$  to  $41^\circ \text{ N}$ ). The maximum depth of the model was 5500 m and it was divided into 39 layers. The model bathymetry is ETOPO1. The Hybrid Coordinate Ocean Model (HYCOM) monthly mean data GLBu0.08 served as the open boundary conditions of the model. Data from 8 main tidal components in TPXO7.2, the global ocean tidal model, were added to the lateral open boundary conditions. Respectively, the output spatial resolution and time interval, include ocean current and sea temperature, are  $0.04^\circ$  ( $\sim 4.4 \text{ km}$ ) and 30 minutes.

The simulated current and SST maps corresponding to the image is presented in figures 2a and 2b, the black rectangles represents the spatial coverage of the SAR-image. We also used the National Center for Atmospheric Research (NCAR) NCEP Climate Prediction System Version 2 (CFSv2) Open Access to Current Data at  $0.5^\circ \times 0.5^\circ$  grids to validate the model-simulated current field, as shown in figure 2c. The model-simulated current fields are more detailed than that from the CFSv2 data. The dark areas in S-1 SAR image is likely to be cold eddy, due to the direction of spiral current. It refers the third generation numeric wave model to as WAVEWATCH III model. The ECMWF data of wind at  $0.125^\circ$ , it was taken as the mandatory wind field

and sounding data was taken from ETOPO1. Respectively, the spatial resolution and time interval output  $0.05^\circ$  ( $\sim 5.5$  km) and 30 min, include current and SST. The simulated significant wave height for the image is shown in figure 2d, indicating that these two images are at low sea state.

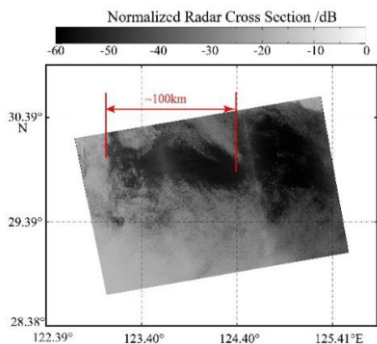


**Figure 1.** VV-polarization S-1 SAR-Image taken around the Zhoushan Island on November 12, 2015, at 09:45 UTC.

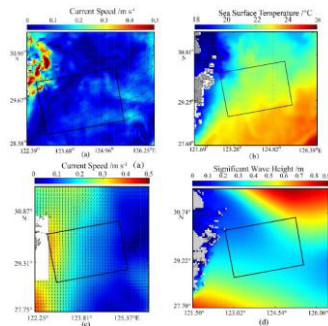


**Figure 2.** (a) The current speed map from Region Ocean Modeling System (ROMS) represents, (b) The AVHRR sea surface temperature map from the ROMS model, (c) The CFSv2 current map, (d) The WW3-simulated significant wave height map. The black rectangles represent the spatial coverage of the SAR image on November 12, 2015, at 09:30 UTC around Zhoushan Island.

### 3. Results

We first present the validation of the model-simulated current and SST against the CFSv2 and the AVHRR data, respectively. It's important to note that the selected area is compared, was set at  $120^\circ$  E to  $130^\circ$  E and  $20^\circ$  S to  $32^\circ$  N. The root mean square error (RMSE) of the model-simulated current speed was 0.04 m/s, shows in figures 3a, whereas figure 3b shows that the RMSE of the model-simulated SST was less than  $2^\circ\text{C}$ . Under such instance, the model-simulated results were considered to be reliable for our study.

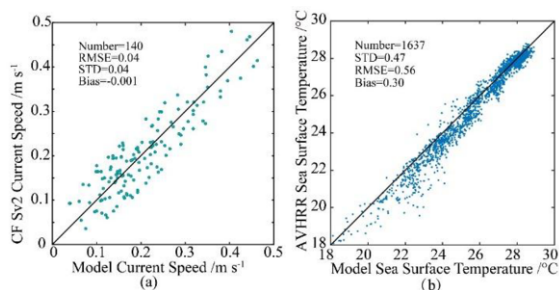


**Figure 3.** (a) The scatter comparison between the CFSv2 data and the model-simulated current speed, (b) The scatter comparison between AVHRR data and the model-simulated sea surface temperature.

In this study, the whole image was divided into several sub-scenes,  $32 \times 32$  at the azimuth and range, and then the auxiliary data, such as wind vector of ECMWF, model-simulated current vector, CFSv2 current, SST, and significant wave height, was bilinearly interpolated at the sub-scenes. There were more than sixty thousand matchups for S-1. As shown in figures 4, the four coloured lines represent the sample lines crossing the dark patterns region. The tendency at all incidence angles between the SAR-measured NRCS with SST was consistent, which was observed as a ‘V’ shape. The wind speed was linearly related with the VV-polarization NRCS; however, the SAR-measured NRCS was greatly affected by wind speed in the upwelling and cold eddy regions. This kind of behaviour was also true for the relation between NRCS and significant wave height, as shown in figure 4a. This is because NRCS is positively related to the significant wave height. The case shown in Figure 4f represents mesoscale cold eddy, and it was found that the current will likely affect NRCS, especially when the current direction changes significantly. The change of NRCS was not closely related with the current speed. Therefore, we hold the view that natural biogenic slicks contributed to the damping Bragg waves associated with the sub-mesoscale upwelling.

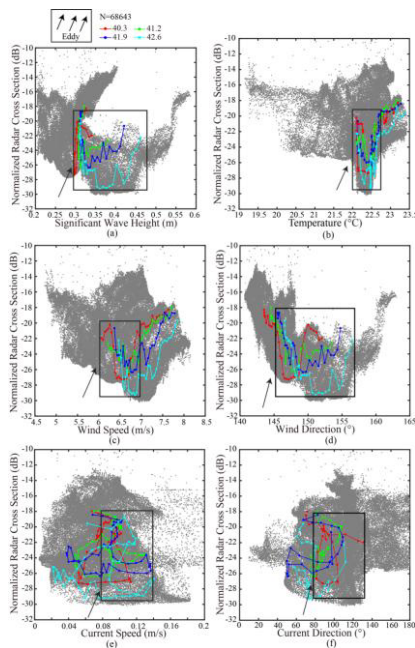


**Figure 4.** The relation between the normalized radar cross section of S-1 SAR and several variables: (a) WW3-simulated significant wave height, (b) AVHRR sea surface temperature, (c) ECMWF wind speed, (d) ECMWF direction, (e) CFSv2 current speed, and (f) CFSv2 current direction.

#### 4. Conclusion

Upwelling and eddy are interesting themes of the marine science community, especially the upwelling occurrence as related to other dynamic processes such as current, wind, and SST on the sea surface. The SAR is a unique technology to observe

sea surface with large spatial coverage, especially for ocean upwelling and eddies. The SST and current fields were simulated simultaneously by using the ROMS model. The validation of SST against AVHRR, as well as the current speed against CFSv2, showed a RMSE around 1 °C and RMSE of 0.04 m/s, respectively.

The AVHRR with model-simulated current data was used to verify the upwelling occurrence. The results showed that the dark patterns in the SAR-images corresponded to low SST region with less change of current direction. The horizontal length of the dark patterns was about 100 km (mesoscale) in S-1 SAR-image, which was probably caused by cold eddies. We concluded that natural biogenic slicks mainly contributed to damping Bragg waves for sub-mesoscale upwelling, however, the ocean current is a very important factor on the sea roughness change for mesoscale cold eddies.

Later, we want to get more SAR images including upwelling and tune a delicate correction model. Furthermore, the model can be implemented for wave and wind retrieval from SAR images.

## References

- [1] Sydeman WJ, García-Reyes M, Schoeman DS, Rykaczewski RR, Thompson SA, Black BA and Bograd S. Climate change and wind intensification in coastal upwelling ecosystems. *Science*. 2014 Jul; 345(6192): 77-80.
- [2] Fragiaco C and Parmiggiani F. An upwelling event in the central mediterranean sea detected by Quikscat and by AVHRR. *International Journal of Remote Sensing*. 2002 Dec; 23(24): 5151-5153.
- [3] McClain CR, Pietrafesa LJ and Yoder JA. Observations of gulf stream-induced and wind-driven upwelling in the georgia bight using ocean color and infrared imagery. *Journal of Geophysical Research Oceans*. 1984 Jun; 89(C3): 3705-3723.
- [4] Sousa FM and Bricaud A. Satellite-derived phytoplankton pigment structures in the Portuguese upwelling area. *Journal of Geophysical Research*. 1992 Jul; 97(C7): 11343-11356.
- [5] Li XM, Chi L, Chen X, Ren YZ and Lehner S. SAR observation and numerical modeling of tidal current wakes at the East China Sea offshore wind farm. *Journal of Geophysical Research Oceans*. 2014 Aug; 119(8): 4958-4971.
- [6] Ding YY, Zuo JC, Shao WZ, Shi J, Yuan XZ, Sun J, Hu JC and Li XF. Wave parameters retrieval for dual-polarization c-band synthetic aperture radar using a theoretical-based algorithm under cyclonic conditions. *Acta Oceanologica Sinica*. 2019 May; 38(5): 21-31.
- [7] Alpers W. Theory of radar imaging of internal waves. *Nature*. 1985 Jan; 314(6008): 245-247.
- [8] Chang J, Huang W, Lou X, Fan K and Shi A. Research on upwelling region wind speed correction method for wind retrieval from SAR imagery along the Zhejiang Coast. *Proceedings of SPIE - The International Society for Optical Engineering*; 2011 Oct. DOI: 10.1117/12.897930.
- [9] Beal RC. A significant post-launch calibration experiment for the SEASAT-A SAR. *Proceeding of Synthetic Aperture Radar Technology Conference*; 1978 Jan.
- [10] Kudryavtsev VN, Grodsky SA, Dulov VA, Malinovsky VV. Observations of atmospheric boundary layer evolution above the gulf stream frontal zone. *Boundary-Layer Meteorology*. 1996 Apr; 79(1): 51-82.
- [11] Johannessen JA, Shuchman RA, Digranes G, et al. Coastal ocean fronts and eddies imaged with ERS-1 synthetic aperture radar. *Journal of Geophysical Research*. 1996 Mar; 101(C3): 6651.
- [12] Marmorino GO, Jansen RW, Valenzuela GR, et al. Gulf stream surface convergence imaged by synthetic aperture radar. *Journal of Geophysical Research Oceans*. 1994 Sep; 99(C9): 18315-18328.
- [13] Friehe CA, Shaw WJ, Rogers DP, Davidson KL, et al. Air-sea fluxes and surface layer turbulence around a sea surface temperature front. *Journal of Geophysical Research Oceans*. 1991 May; 96(C5): 8593-8609.
- [14] Clemente-Colon P and Yan XH. Observations of east coast upwelling conditions in synthetic aperture radar imagery. *IEEE Transactions on Geoscience and Remote Sensing*. 1999 Oct; 37(5): 2239-2248.